ADVANCED ENERGY MATERIALS
www.advenergymat.de

Design Rules for Polymer Blends with High Thermoelectric Performance

*Osnat Zapata-Arteaga, Sara Marina, Guangzheng Zuo, Kai Xu, Bernhard Dörling, Luis Alberto Pérez, Juan Sebastián Reparaz, Jaime Martín, Martijn Kemerink, and Mariano Campoy-Quiles**

A combinatorial study of the effect of in-mixing of various guests on the thermoelectric properties of the host workhorse polymer poly[2,5-bis(3-tetradecylthiophen-2-yl)thieno[3,2-b]thiophene] (PBTTT) is presented. Specifically, the composition and thickness for doped films of PBTTT blended with different polymers are varied. Some blends at guest weight fractions around 10–15% exhibit up to a fivefold increase in power factor compared to the reference material, leading to *zT* values around 0.1. Spectroscopic analysis of the charge-transfer species, structural characterization using grazing-incidence wide-angle X-ray scattering, differential scanning calorimetry, Raman, and atomic force microscopy, and Monte Carlo simulations are employed to determine that the key to improved performance is for the guest to promote long-range electrical connectivity and low disorder, together with similar highest occupied molecular orbital levels for both materials in order to ensure electronic connectivity are combined.

1. Introduction

Organic semiconductors are promising candidates for thermoelectric materials due to their low cost, abundant main constituting elements, and good scalability onto commercially available printing techniques. The performance of these materials is benchmarked with the figure of merit $ZT = \frac{\sigma S^2}{\kappa} T$, where σ is the electrical conductivity, S is the Seebeck coefficient, κ is the thermal conductivity, and T is the absolute temperature. However, a long-standing problem for optimizing the zT lies in the interplay between S and σ with carrier concentration (η). That is, whereas σ increases as a function of η and carrier mobility μ, the parameter S scales inversely with η. Thus, a significant amount of effort relies on fine-tuning η via doping to find the best performance for a given semiconductor and dopant pair.

Alternatively, other methods aim to improve σ through μ by increasing the network's long-range connectivity and mean free path, e.g., through rubbing, stretching, annealing, and other morphology-control processing techniques.[1–4] These methods, depending on the obtained degree of order and anisotropy, can benefit thermoelectric performance. For example, in highly anisotropic rubbed polymer films, it is possible to

O. Zapata-Arteaga, K. Xu, B. Dörling, L. A. Pérez, J. S. Reparaz, M. Campoy-Quiles
Institute of Materials Science of Barcelona
ICMAB-CSIC
Campus UAB
Bellaterra CP 08193, Spain
E-mail: mcampoy@icmab.es

S. Marina, J. Martín
POLYMAT and University of the Basque Country
Av. de Tolosa 72, Donostia-San Sebastián 20018, Spain

G. Zuo
Institute for Physics and Astronomy
University of Potsdam
14476 Potsdam-Golm, Germany

The ORCID identification number(s) for the author(s) of this article can be found under https://doi.org/10.1002/aenm.202104076.

© 2022 The Authors. Advanced Energy Materials published by Wiley-VCH GmbH. This is an open access article under the terms of the Creative Commons Attribution License, which permits use, distribution and reproduction in any medium, provided the original work is properly cited.

DOI: 10.1002/aenm.202104076

J. Martín
Grupo de Polímeros
Centro de Investigacións Tecnolóxicas (CIT)
Universidade da Coruña
Esteiro, Ferrol 15471, Spain

J. Martín
Ikerbasque
Basque Foundation for Science
Bilbao 48013, Spain

M. Kemerink
Centre for Advanced Materials
Heidelberg University
Im Neuenheimer Feld 225, 69120 Heidelberg, Germany

M. Kemerink
Division of Electronics and Photonic Materials
Department of Physics
Chemistry and Biology
Linköping University
Linköping 58183, Sweden

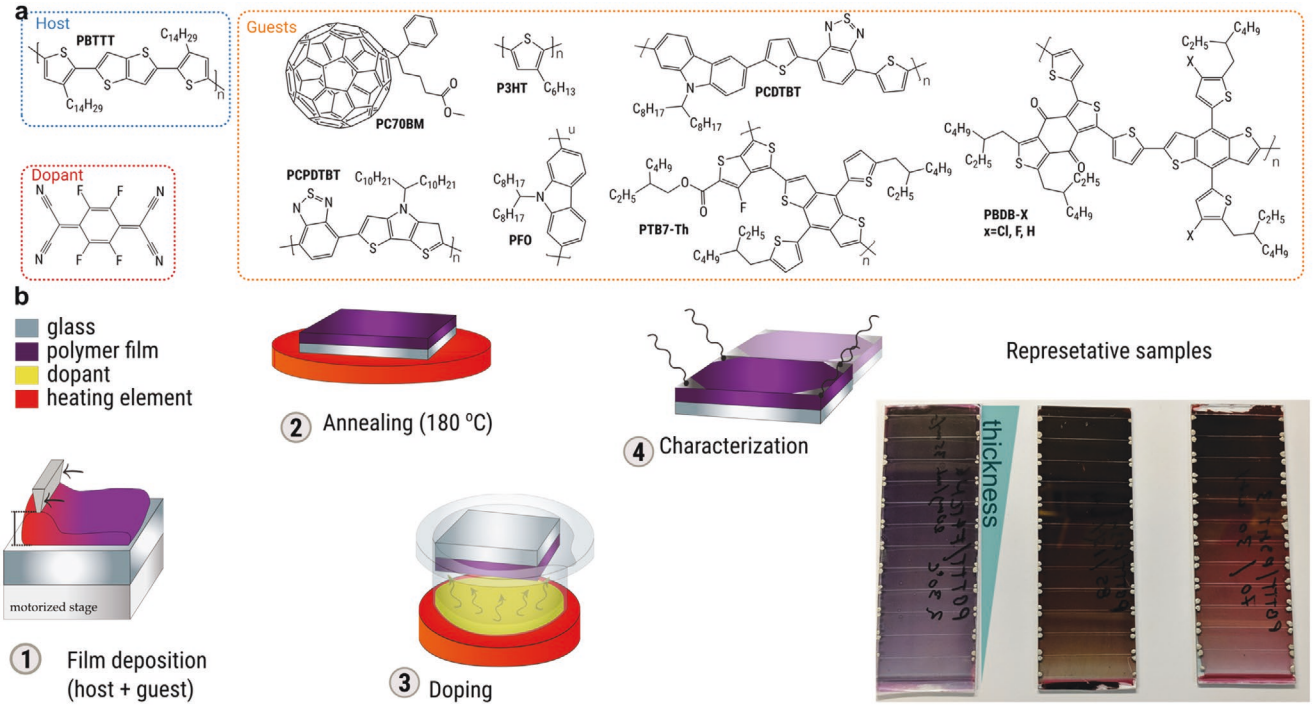

Figure 1. a) Chemical structures of the host, dopant, and guest materials utilized throughout this work. b) General scheme of the fabrication, doping and post processing methodology followed on each sample. Also for clarity, a representative picture of films with a thickness gradient.

partially decouple the S–σ relationship by forcing carriers to hop along a preferential direction, leading to an σ and S that scale with the degree of anisotropy.[3] A similar effect can occur within the density of states (DOS) engineering framework, which comprises mixtures of polymer semiconductors to modify the energy landscape.[5–8] Given that in a Gaussian-shaped DOS describing the highest occupied molecular orbital (HOMO) and lowest unnocupied molecular orbital (LUMO), charge transport can be modeled to occur through characteristic hopping events between the Fermi Energy E_F and sites close to the transport energy E_{tr}, where $S \approx (E_F - E_{tr})/T$. For a mixture of polymer semiconductors of adequately chosen energy levels and composition, the Gaussian DOS can split into two peaks, effectively widening the gap between E_F and E_{tr} and thus leading to an increase in S. It has been shown that within a narrow composition range, S can even exceed that of the pure materials.[7]

However, the techniques mentioned above have some underlying issues. For example, rubbing or stretch-alignment may not be compatible with all classes of semiconducting polymers or scaled-up manufacturing techniques. Moreover, the alignment techniques used so far are limited to thin films of limited practical use in thermoelectrics. On the other hand, the DOS engineering approach investigated so far focused on having a main transport polymer mixed with a second polymer that could not be doped for the given used dopant. In that case, the double peak DOS tends to appear at fractions farther away from the best-conducting polymer fraction. In addition, this approach is rather sensitive to the degree of phase separation between host and guest materials. Due to these factors, charge transport occurs within a handful of conducting domains in a sea of "electrically insulating" domains.[9] This causes a substantial penalty in σ, thus limiting any benefit on the zT.

Inspired by the DOS approach, we chose to investigate the case of two polymer semiconductors with only a small difference in their energy levels, amenable to be doped with the same dopant and thus, hoping to achieve some degree of splitting in the DOS while simultaneously reducing the amount of electrically insulating domains within the network.

Specifically, we investigated F4TCNQ-doped blends composed of poly[2,5-bis(3-tetradecylthiophen-2-yl)thieno[3,2-b]thiophene] (PBTTT)-host and a series of guest organic semiconductors, namely P3HT, [6,6]-Phenyl-C71-butyric acid methyl ester (PC70BM), poly(9,9-di-n-octylfluorenyl-2,7-diyl) (PFO), PTB7-Th, PCDTBT, PCPDTBT, PBDB-T, PBDB-2F, and PBDB-2Cl (see **Figure 1**). We demonstrate that for some of the polymers and in particular P3HT and PTB7-Th at concentrations from 10 to 15 wt% lead to a fivefold increase in the power factor compared to the pure F4TCNQ-doped PBTTT samples. Through UV–vis–NIR spectroscopy and kinetic Monte Carlo simulations (kMC), we determine that our observations do not follow a pure modulation of the doping level nor engineering of the DOS. The latter compelled us to study the film structure using grazing-incidence wide-angle X-ray scattering (GIWAXS) and the morphological changes using atomic force microscopy (AFM). We find that the blends with 10 wt% of P3HT are textured along a preferential direction and have a morphology that resembles the more ordered ribbon phase of pure PBTTT normally accessed after annealing at high temperatures. Our results indicate that the thermoelectric improvement is due to a synergistic effect where the guest enhances the morphology and structural order of the host and, simultaneously possesses a HOMO level

© 2022 The Authors. Advanced Energy Materials published by Wiley-VCH GmbH

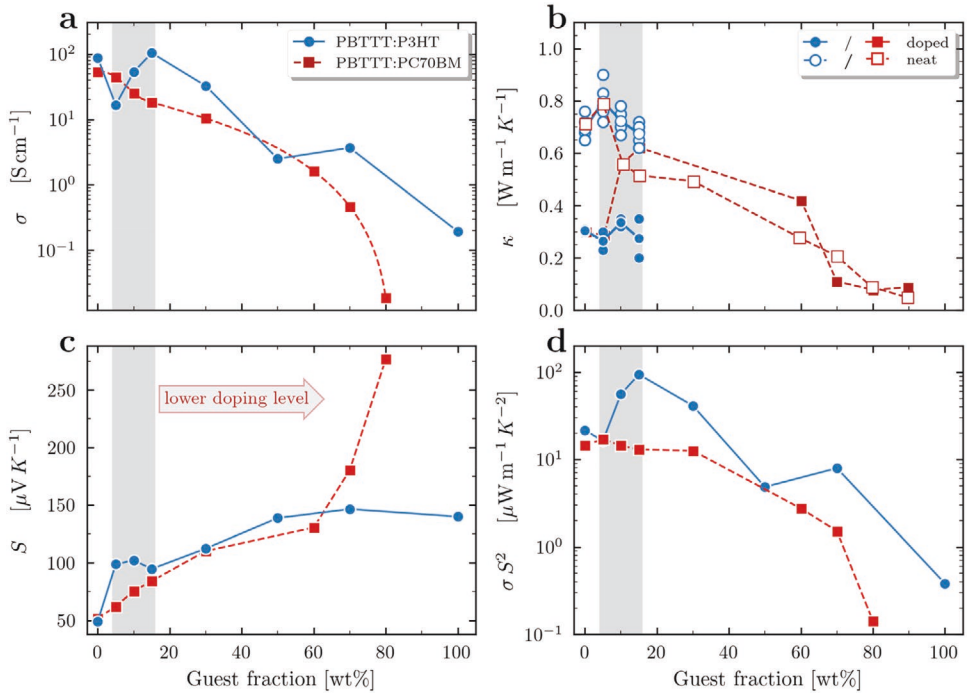

Figure 2. Thermoelectric properties for films of PBTTT with varied fractions of P3HT and PC70BM. a) Electrical conductivity, b) thermal conductivity, c) Seebeck coefficient, and d) power factor. The gray area highlights the region with a simultaneous increase in the electrical conductivity and Seebeck coefficient when using P3HT as the guest material.

close to that of the host material to facilitate charge transport across the network.

2. Results and Discussion

To study the dependence of the thermoelectric properties on the microstructure and composition of polymer blends, we fabricated three groups of samples: i) A baseline group comprising pure PBTTT, hereafter referred to as "reference." ii) A group composed of PBTTT with varying fractions of P3HT (guest), which are studied in greater detail. iii) A group composed of PBTTT with varying fractions of other guest materials, namely, PC70BM, PTB7-Th, PFO, PCPDTBT, PCDTBT, PBDB-T, PBDB-2F, and PBDB-2Cl.

We employed group ii to study a scenario where both the host and guest materials have relatively similar energy levels, thus to facilitate a charge-transfer process with F4TCNQ, and group iii, to determine whether the structural or energetic properties of the studied guest materials are responsible for our observations. Postprocessing steps were identical for all groups of samples. Specifically, thermal annealing at 180 °C for 15 min, followed by doping with F4TCNQ using a vapor-phase methodology described in a previous publication.[10] Also, to study a larger pool of comparable samples, we fabricated several host: guest pairs with a gradient in thickness to characterize them locally. This high-throughput-like approach enables us to investigate the role of thickness while reducing batch-to-batch variations in a number of samples that would be equivalent to ≈190. Figure 1 shows the chemical structures of said materials and illustrates the general methodology (see experimental section and Supporting information for additional details).

Figure 2 presents the thermoelectric properties of thin films (≈40 nm) of PBTTT as a function of the guest fraction of P3HT and PC70BM. For blends of PBTTT: P3HT, σ and S exhibit two regimes. 1) An overshoot between 5 and 15 wt% and 2) followed by a reduction in σ above 15 wt% with a relatively insensitive change in S (cf. Figure 2a,c). In the first regime (1), σ drops to a lower value than the reference and then increases linearly with increasing P3HT content, reaching ≈100 S cm^{-1} for guest fractions of 15 wt%. Interestingly, we observe a similar increasing trend in S within the same regime, which typically should *not* occur unless accompanied by a significant decrease in σ. In the second regime, further addition of the guest material lowers σ by almost three orders of magnitude and improves the Seebeck coefficient by approximately a factor of three compared to the reference. Also noteworthy is a small increase in κ for the 5, 10, and 15 wt% compositions compared to the reference. This change is intriguing because it occurs in the *neat* (undoped) reference films, thus discarding any electronic contribution effect from doping and pointing toward a change in the material's microstructure. Upon doping, the thermal conductivity decreases due to additional scattering of vibrations from the dopant molecules, as previously shown for F4TCNQ doped PBTTT.[11] Although σ at 15 wt% is only marginally different from the reference, the power factor is significantly higher due to its dependence on S squared. Moreover, even though the presented trend is more pronounced in thin films, we observe the same behavior for a significant number of measurements regardless of the film's thickness and also when using

© 2022 The Authors. Advanced Energy Materials published by Wiley-VCH GmbH

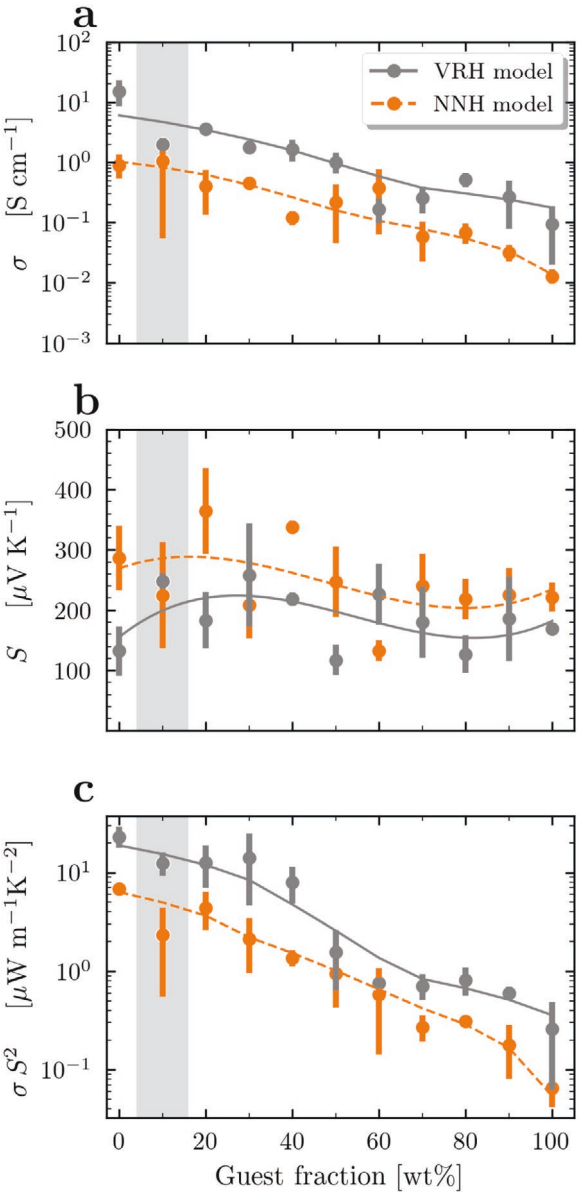

Figure 3. Results of kinetic Monte Carlo simulations of different compositions of PBTTT: P3HT using variable range hopping (VRH) and nearest-neighbor hopping (NNH). a) Electrical conductivity, b) Seebeck coefficient, and c) power factor. Note that the simulations do not show a peak performance between 5 and 15 wt%, as in the experimental results (cd. Figures 2 and 3). Simulations were performed with the following parameters: Gaussian energetic disorder σ_{DOS} = 50 meV, temperature T = 300 K, intersite distance α_{NN} = 1.8 nm, attempt frequency $\nu_0 = 1 \times 10^{13}$ s^{-1}, energy offset of dopant ΔE = 50 meV, doping concentration c = 0.08.

a spin coating instead of blade coating (Figure S1, Supporting Information).

In contrast, we present a case where a mixture of two organic semiconductors exhibits the commonly observed tradeoff between σ and S due to a modulation of the doping level.[12–14] Here, doped blends of PBTTT: PC70BM show a monotonous decrease in σ accompanied by an increase in S. For this mixture, the observed behavior can be understood as follows: Mixtures of PBTTT: PC70BM form a bimolecular crystal where the fullerene intercalates between the sidechains of the polymer.[15,16] Similarly, for F4TCNQ-doped P3HT and PBTTT, the dopant also allocates between the sidechains of the polymer.[17–19] Thus, we can conclude that the dopant has fewer available doping sites within the intercalated PBTTT: PC70BM crystal, which has a direct impact on the doping level of the film. The presence of the polymer: fullere bimolecular crystal also has an impact κ. For *neat* mixtures of PBTTT: PC70BM, κ increases with guest fractions of 5 wt %. Further addition of the fullerene fraction leads to decreasing κ values that tend to that of the pure fullerene fraction, thus, similar to what one would expect in a rule of mixtures. Upon doping, there is a sharp decrease in κ with 5 wt% of PC70BM, followed by a threefold increase for fractions between 10 and 60 wt%. Notably, values of κ for fullerene fractions above 5 wt% are similar to that of the neat mixture. Such similarity can be rationalized to a low amount of F4TCNQ capable of introducing thermal scattering. The trends in κ from this section suggest possible pathways to tune the thermal conductivity in organic semiconductors but, more importantly, suggest that the slight increase in κ for PBTTT: P3HT between 5 and 15 wt% is related to changes in the structural order, as seen in the case of the PC70BM mixtures.

Arguably, the peak performance found at 15% for the PBTTT: P3HT composition mimics to some degree the DOS engineering effects described by Zuo et al.[7] Nevertheless, we consider the energy levels of PBTTT and P3HT as being too similar for creating a well separated double-peak DOS (see Table S1 and Figure S2, Supporting Information). To understand the specific scenario, we performed kinetic Monte Carlo simulations, which were previously demonstrated to adequately reproduce the physics governing the thermoelectric properties in organic semiconductors.[7] In **Figure 3**, we present the simulated thermoelectric properties of PBTTT with varying fractions of P3HT using nearest-neighbor hopping (NNH) and variable range hopping (VRH) models. Both indicate a monotonous decrease in conductivity with increasing P3HT content and a relatively insensitive thermopower. In other words, the simulations cannot reproduce the experimental results, corroborating that a different explanation for the improved thermoelectric performance is required.

2.1. Effect of the Doping Level on the Thermoelectric Properties of Polymer Blends

To get further insight into the doping level of the studied films, we performed UV–vis–NIR spectroscopy measurements and fitted the characteristic bands of the charge-transfer species. **Figure 4**a shows the UV–vis–NIR spectra for different compositions of doped PBTTT: P3HT and Figure 4b,c presents the analysis of the characteristic bands of the F4TCNQ anion and charge transfer complex (CTC) species (see characterization section and Figure S3, Supporting Information).[10,17–20] The comparison of Figure 4a–c shows that the addition of P3HT induces the formation of more CTC species than in the reference. At the P3HT concentrations of 5 and 50 wt%, the CTC presence is significant and coincides with those concentrations exhibiting a larger drop in σ (as seen in Figure 3d), likely due to

© 2022 The Authors. Advanced Energy Materials published by Wiley-VCH GmbH

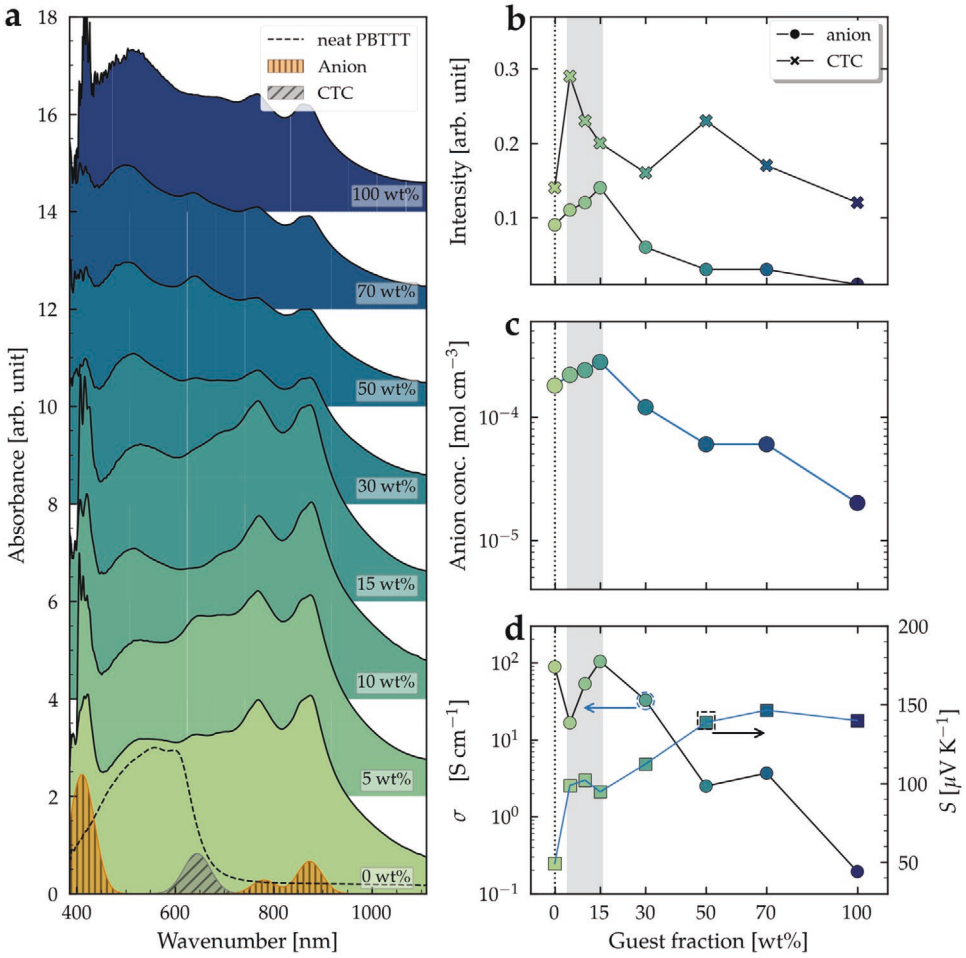

Figure 4. a) UV–vis–NIR absorbance spectrum of doped PBTTT for different fractions of P3HT. Also included, the spectrum of neat PBTTT and the contributions of F4TCNQ anion and CTC species of a selected sample. b) Band intensity for the F4TCNQ anion (790 nm) and the CTC (630 nm) extracted from the fitted spectrum. c) Calculated F4TCNQ anion concentration and d) measured electrical conductivity and Seebeck coefficient for the 40 nm films introduced in Figure 2.

the relatively inefficient free-carrier generation from CTC.[20,21] On the other hand, from 5 to 15 wt%, anion content increases linearly with the amount of guest material, indicating a higher anion concentration for these compositions than in the reference material (as seen in Figure 4b).

We note that estimating the anion concentration from the absorbance spectrum reveals anions distributed within the entire blend. Moreover, this method lacks the sensitivity to differentiate the percentage contained in a specific polymer fraction due to the spectral overlap between the features of the two polymers. Thus, it is possible that a portion of the generated charge-transfer species originates from P3HT and that we overestimate the actual doping level of the dominant percolating network. Furthermore, we can speculate that P3HT is easier to dope based on the following. P3HT has an easier-to-oxidize tail of density of states for an integer charge transfer process to occur than PBTTT.[17,22] As F4TCNQ fills these states, the dopant then proceeds to populate the remaining sites of P3HT primarily through CTC formation.[17,22] At low and intermediate guest fractions, the number of these easier-to-oxidize density of states in P3HT is limited compared to the entire density of states in the whole polymer network. One would then expect an elevated proportion of CTC states, which is what we observe upon blending. In this sense, we could expect an overestimation of the dopant concentration of PBTTT, particularly at low P3HT fractions. By contrast, the anion concentration drops below the reference value for the second regime (above 15 wt%) and mimics the trend observed in σ presented in Figure 4d. Thus, the present observations cannot corroborate a lower doping level in the blends' polymer network, but they may indicate that a part of the observed anion species corresponds to the doped P3HT fraction. Notably, the analysis of the doping level does not provide evidence that the increase in the Seebeck coefficient upon adding small amounts of P3HT is related to a decrease in the charge carrier density.

2.2. Structural Characterization

A different way to rationalize our results is by invoking a structure-related enhancement of the thermoelectric properties. As mentioned above, recent publications indicate that structural

© 2022 The Authors. Advanced Energy Materials published by Wiley-VCH GmbH

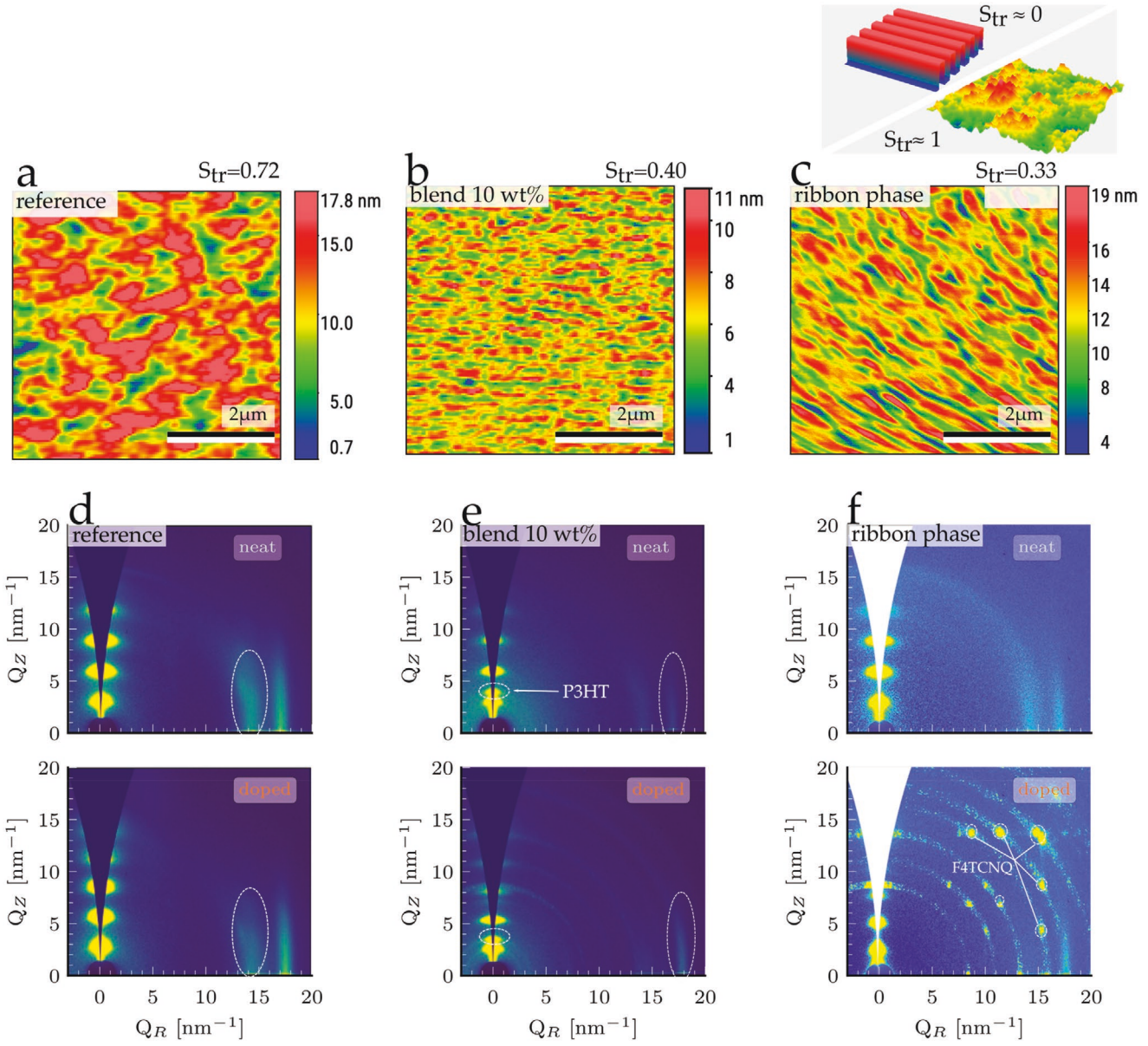

Figure 5. AFM topography images for doped- a) pure PBTTT annealed at 180 °C, b) a 10 wt% blend annealed at 180 °C, and c) pure PBTTT annealed at 270 °C. The upper inset shows the texture aspect ratio (Str), where features in a surface with a dominant orientation have a value close to 0, whereas a spatially isotropic texture will result in a Str of 1. (d)–(f) present the 2D GIWAXS patterns for the neat (top) and corresponding doped samples (bottom).

anisotropy can lead to a simultaneous increase in S and σ in highly crystalline polymers.[3,23–25] Scheunemann et al. ascribed this phenomenon to carriers being forced to hop along a preferential direction, modifying the transport energy E_{tr}, and thus S through $S \propto \frac{E_F - E_{tr}}{T}$.[3] Alternatively, one may obtain a simultaneous increase in S and σ if the charge carrier density in the part of the blend through which transport occurs is reduced (potentially increasing S), together with a large increase in the charge carrier mobility that compensates the fewer number of charges, resulting in larger σ values. As both scenarios are related to the film's microstructure, we performed a detailed morphological characterization to pinpoint changes occurring in the morphology and microstructure of the polymer blend materials.

Figure 5a–c shows the topography images for three doped selected samples: The reference, a 10 wt% blend, and for comparison, pure PBTTT in the ribbon phase. The latter is obtained when films are processed at much higher temperatures than those used in this work (see below). The reference shows the typical "terraces" reported for PBTTT when annealed at temperatures between 160 and 180 °C, corresponding to the melting of the alkyl side chains. These terraces have lateral dimensions that range from 200 to 1000 nm and step heights from 2 to 6 nm, which agrees reasonably well with previous reports.[26–29] For this sample, the texture aspect (S_{tr}) ratio is close to 1, indicating that the film is *not* textured along a preferential direction. In contrast, the 10 wt% blend has thinner terrace-like features with a preferential orientation, as

© 2022 The Authors. Advanced Energy Materials published by Wiley-VCH GmbH

noted by a lower texture aspect ratio. This phenomenon does not occur in blends with higher P3HT content. For example, in the 30 and 50 wt% compositions, the morphology becomes more isotropic, and the texture aspect ratio goes back toward 1 (as seen in Figure S4, Supporting Information). Arguably, the morphology of the 10 wt% blends resembles the more ordered ribbon phase of PBTTT that appears after annealing temperatures above 240 °C (cf. Figure 5a–c), that is associated with the melting of the backbone.[30,31] Here, the ribbon-like features orient perpendicular to the fluid flow direction and comprise extended polymer backbones across the width of the ribbon.[4,30,32] We highlight that both the reference and blend groups were processed at 180 °C, *well below* the temperature required for a transition into the ribbon phase of pure PBTTT. Thus, the changes in morphology observed for the 10 wt% blends are linked to the components in the ternary composition (i.e., P3HT or F4TCNQ) with and not solely arising from temperature. Thus, one might think of P3HT inducing an effect similar to a melting point depression. That is, blending may reduce the chemical potential of the ribbon phase so that the ribbon phase becomes stable at a lower temperature.[33,34]

We have performed fast scanning calorimetry (FSC) measurements to test this hypothesis (Figures S5 and S6, Supporting Information). Comparing the neat PBTTT and the blend with 15 wt% of P3HT, we do not observe a clear depression in the endothermic peak associated to the transition to the ribbon phase. This may be related to a low degree of miscibility between the two materials, or, alternatively, similar chemical potentials of neat and blended materials. In another set of experiments, we determined the glass transition temperatures of neat and blend films, showing that this lies around 80 °C, and thus the current annealing protocol at 180 °C will likely result in polymer: polymer demixing. The remaining question would be if the ribbon phase is facilitated upon doping. Unfortunately, we are not able to evaluate any thermal transition depression in the ternary mixture (i.e., host, guest, and dopant), since F4TCNQ has a very limited thermal stability. We will come back to this point below.

The consequences of a better structural order and orientation on the charge transport properties of PBTTT are significant. For example, the field-effect transistor mobility reported for the ribbon phase can be up to an order of magnitude higher than that of as-cast films of PBTTT.[28,29,32] Concomitantly, films of PBTTT with better structural order or some degree of orientation tend to show higher values in σ.[18,23,25] Indeed, our AFM current maps agree with such observations and with the macroscopic electrical measurements presented earlier (cf. Figure 2 and Figure S7, Supporting Information); By adding 10 wt% of P3HT, the morphology becomes more ordered, and more conductive than the reference as suggested by the topography and current-sensing AFM experiments (cf. Figures S4 and S5, Supporting Information). The opposite occurs in blends with 30 or 50 wt% of P3HT, the film becomes more isotropic and less conductive. These observations also align with the slight increase in κ observed in neat blends of PBTTT: P3HT for 5, 10, and 15 wt%.

In order to further evaluate the microstructure of pure and blend films, we performed GIWAXS measurements to understand the structural difference between the reference, a 10 wt% blend, and PBTTT in the ribbon phase. Figure 5e,f, presents the 2D GIWAXS patterns for the neat and doped samples mentioned above (for the integrated patterns see Figure S8, Supporting Information). Neat PBTTT orients in an edge-on configuration where the out-of-plane scattering features across the in-plane direction correspond to the lamella-stacked sidechains and the in-plane scattering features along the out-of-plane direction, to the backbone chain and the π–π-stacking (14.2 and 17.1 nm^{-1}, respectively).[18,22,35,36] We highlight that the ribbon phase of pure PBTTT has the same structure and texture as the reference but possesses a shorter π–π-stacking distance and a larger lamella-stacked distance. The neat 10 wt% blend shows the same scattering features as the reference and an additional scattering feature at Q_Z = 3.8 nm^{-1}. Based on its position and intensity, we ascribe the latter to the P3HT fraction.[37] This blend also shows a weaker scattering intensity at 14.2 nm^{-1}, yet it is unclear if the origin is related to disorder across the backbone chain or a thickness difference compared to the reference. Besides these changes, the scattering features in the blend shift slightly or broaden in some cases, but no new *strong* scattering features emerge as one may expect if cocrystallization or a different polymorph were to occur.[16,20]

By contrast, doping induces more evident changes in all samples. The peaks in the out-of-plane direction (q_Z) shift toward shorter scattering vectors Q, while peaks in the in-plane direction (q_R) shift toward larger scattering vectors. For PBTTT, these effects are attributed to F4TCNQ allocating between the sidechains, expanding the lattice while simultaneously inducing a more cofacial configuration between adjacent backbones.[10,11,18,38] Accompanied by these changes, the scattering feature at q_R = 14.2 nm^{-1} decreases in intensity, indicating dopant-induced disorder along the backbone chain direction.[18,20,37] We highlight that previous effects appear to be more pronounced for the ribbon phase and the 10 wt% blend (cf. Figures S8 and S9, Supporting Information). However, an in-depth analysis is complicated due to scattering peaks of excess F4TCNQ accumulated on the film's surface, which overlap with those by the polymer. Furthermore, for the 10 wt% blend, the peak at q_Z = 3.8 nm^{-1} narrows compared to its neat counterpart, indicating more ordered domains as described for P3HT in refs. [37,39] (see Figure S8 and S9, Supporting Information for a comparison and analysis of the GIWAXS patterns). Thus, the present observations indicate that PBTTT retains its structural order when adding 5–10 wt% of P3HT. This agrees well with the FSC experiments (see above). It is only after doping that the lattice of the 10 wt% compositions expand in a manner that resembles more that of the doped ribbon phase rather than the reference material.

Figure S10 in the Supporting Information shows the Raman spectra of doped PBTTT as well as its blends with P3HT and PC70BM. The blend with fullerene, known to produce a cocrystal of the two materials (see above), shows the main vibrations shifting to lower wavenumbers, as it is typically observed when crystallinity is enhanced. On the other hand, blending with P3HT and F4TCNQ positions the Raman peaks at intermediate wavenumbers between the neat PBTTT and the fullerene cocrystal. Raman would also support the previous evidence regarding an enhanced degree of crystallinity induced in the ternary system.

© 2022 The Authors. Advanced Energy Materials published by Wiley-VCH GmbH

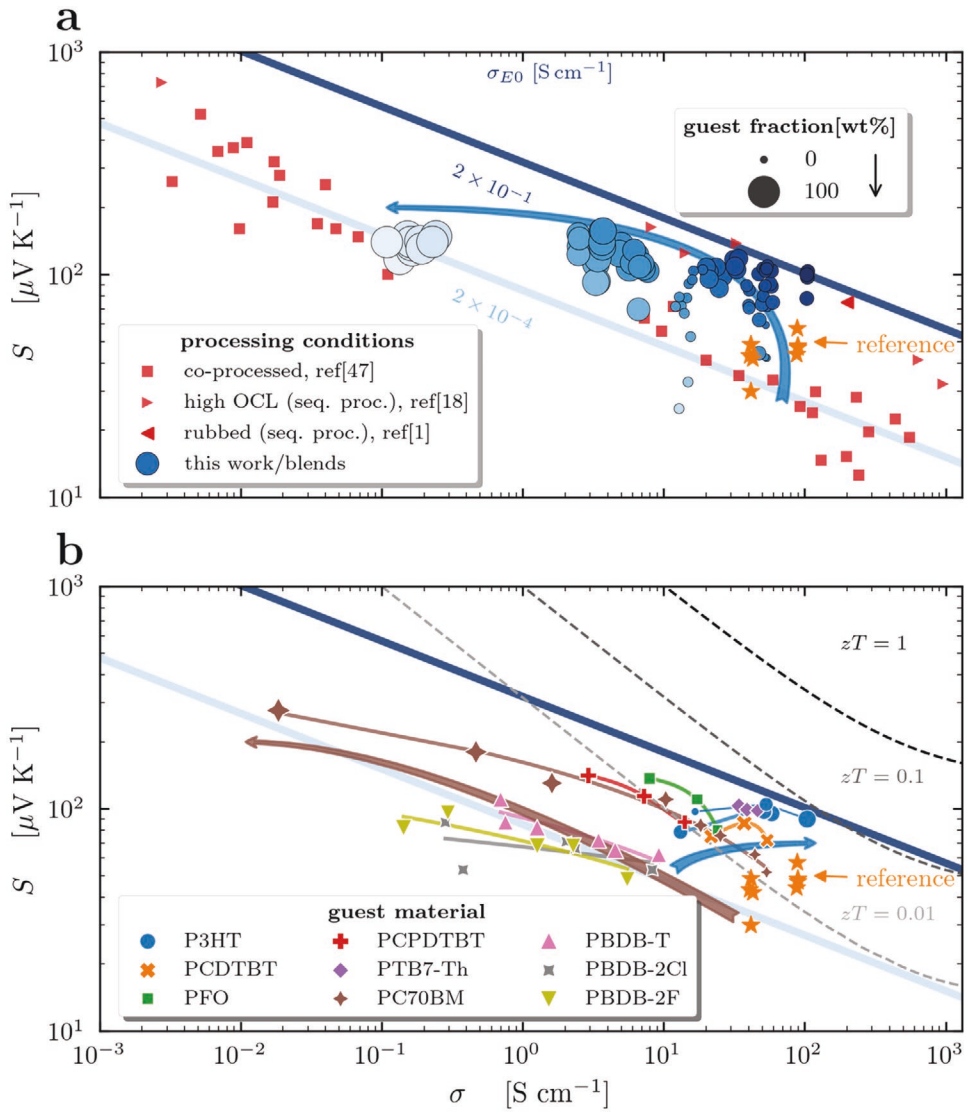

Figure 6. a) Seebeck coefficient as a function of the electrical conductivity. Blue circles correspond to the experimental values of different compositions of PBTTT: P3HT from Figure 2 and Figure S1 in the Supporting Information. The size and color of the circle indicate the guest fraction and σ_{E0} respectively. Red markers correspond to compiled literature data for F4TCNQ-doped PBTTT processed via codeposition[45] for films with a high degree of orientational correlation length (OCL)[18] and oriented films processed via rubbing.[1] b) Seebeck coefficient as a function of the electrical conductivity for films of PBTTT mixed with other guest materials in compositions from 5 to 15 wt%.

2.3. Impact of Blending on Thermoelectric Properties

Because σ varies significantly as a function of the film's structural order even with similar doping levels, assessing its effect on the Seebeck coefficient is crucial. A convenient approach relies on plotting S as a function of σ along with the universal 1/4 power-law relationship proposed by Glaudell et al.[12,37,40] and given in Equation (1).

$$S = \frac{k_B}{q}\left(\frac{\sigma}{\sigma_{E0}}\right)^{-\frac{1}{4}} \quad (1)$$

Here, k_B/q is the Boltzmann constant over the unit charge and σ_{E0} is a fitting parameter that shifts the S–σ curve left or right. The importance of the $S \approx \sigma^{-1/4}$ correlation is that it accommodates the experimental trend observed in many organic semiconductors over a wide range of σ values and that it allows a meaningful performance comparison without necessarily knowing the doping level. On the other hand, σ_{E0} is often regarded as a weighed mobility prefactor[41] or, in other models, to the sample's homogeneity and maximum conductivity of a given conductive domain.[42] Experimental results show that this value is higher in ordered or even oriented materials regardless of the interpretation chosen. Thus, in principle, it can serve as a proxy for the degree of connectivity between conductive domains and structural order. For example, coprocessed films of doped PBTTT have a more disordered structure than sequentially processed rubbed films, and thus, show a lower σ_{E0} for a wide range of electrical conductivities (as seen in **Figure 6**a).[18,43–45]

© 2022 The Authors. Advanced Energy Materials published by Wiley-VCH GmbH

In the results comprising PBTTT: P3HT, we observe a deviation from the $S \propto \sigma^{-1/4}$ curve. Specifically, σ_{E0} increases for guest loads between 0 and 15 wt% and then decreases with higher guest contents. The best-performing compositions (10 and 15 wt%) reach similar values as samples processed through other more sophisticated techniques (as seen in Figure 6 and Figure S11, Supporting Information), e.g., rubbed PBTTT or films with a high length scale of aligned backbones (orientational correlation length, OCL).[1,18,24] Such observations highlight that PBTTT can already display a wide range of S and σ values strictly through changes in the film's microstructure and order. There is further evidence of these trends when comparing the thermoelectric performance of F4TCNQ-doped neat PBTTT crystallized at different temperatures, along with their AFM topography maps (as seen in Figure S12, Supporting Information). With the evidence above, we hypothesize that the addition of P3HT, in our case, acts as a facilitator for the preferred microstructure.

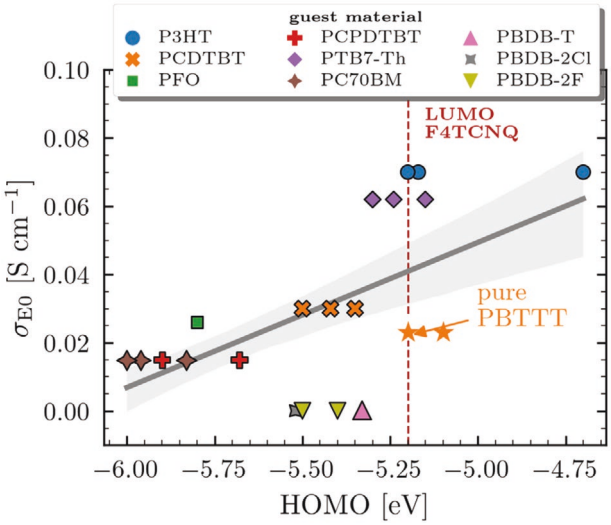

Figure 7. Fitted σ_{E0} as a function of the HOMO level for each related material.

2.4. Extension to Other Materials

This section aims to identify the crucial traits that produce high power factors in blends. So far, we have shown that the addition of P3HT induces beneficial morphological changes in the host polymer. We, however, cannot be sure if this change alone is responsible for our observations in terms of thermoelectric performance. For instance, the UV–vis analysis may indicate that a fraction of the calculated anions is related to the P3HT fraction and thus it is unclear whether these generated carriers contribute to the main percolating network. To rationalize our observed experimental results, we investigated if the favorable energy alignment of the guest material with the dopant F4TCNQ, and thus, a charge-transfer process is required. Following this train of thought, we studied other materials of varied HOMO energy levels (see Table S1 and Figure S2, Supporting Information, for a summary of these materials and their properties). As in the previous case, we employ σ_{E0} to classify their performance and as a "quality marker" for the connectivity and structural order between domains.

In Figure 6b, we present the thermoelectric properties of the samples mentioned above, fabricated with 5, 10, and 15 wt% of the guest material. In this study, we used as guest materials PFO, PTB7-Th, PCDTBT, PCPDTBT, PBDB-T, PBDB-2F, and PBDB-2Cl. As in previous cases, all compositions were post-processed identically, i.e., the same annealing temperatures and doping time were used. For comparison, we also reproduce the experimental trends of PBTTT: PC70BM and PBTTT: P3HT presented in Figure 1. First, we note that all blends exhibit a higher Seebeck coefficient than the reference PBTTT processed in the same conditions. Generally speaking, the electrical conductivity is either maintained or reduced upon blending. As a result, the power factor increases or decreases depending on the specific compromise between these two parameters. Specifically, blends of PBTTT with P3HT, PTB7-Th, and PCDTBT produce an improved performance for some compositions, while the rest of the blends reduce the power factor regardless of the composition.

We highlight that all new blends seem to follow a fixed $S \propto \sigma^{-1/4}$ when varying the guest fraction, like in PBTTT: PC70BM. Nevertheless, each family has a different σ_{E0} offset, which already suggests different degrees of interconnectivity. Further analysis shows that σ_{E0} increases when using guest materials with HOMOs closer to the doping range of F4TCNQ, as seen in **Figure 7**. For example, PTB7-Th appears in the upper section of the trend, followed by PCDTBT, then PCPDTBT, and in the final position PC70BM. Interestingly, analysis of the absorption bands corresponding to the CTC or the integer charge transfer (ICT) for blends of PBTTT and PTB7-Th do not show evidence that the guest materials are getting doped (see Figure S13 and S14, Supporting Information). However, the materials leading to the higher electrical conductivities have HOMOs close to the LUMO of F4TCNQ, suggesting that these guest materials lead to an energy landscape for carriers in the doped PBTTT blend that facilitates or at least does not hamper charge transport. In order words, the barriers for transport might be smaller in these materials than for guests with larger HOMO level offsets. The exceptions to the trends discussed above are PBDB-T, PBDB-2F, and PBDB-2Cl, which, according to their energy levels, one would expect to behave similarly to PCDTBT. However, they show very modest performance. This could be due to them having less planar structures that could affect morphology and structural order in PBTTT. For example, the fact that PFO does not result in a statistically meaningful improved performance can be tentatively ascribed to its small size, which does *not* disturb the microstructure of PBTTT (as seen in Figure S15, Supporting Information), even though has a far deeper HOMO. So, the comparison thus far indicates that having well aligned energy levels is necessary but not enough for a performance improvement. Nonetheless, understanding the mechanism by which P3HT enhances the morphology of PBTTT is complicated. We speculate that the ternary system formed by adding both P3HT and F4TCNQ may cause a reduction of the terrace-to-ribbon transition compared to the

© 2022 The Authors. Advanced Energy Materials published by Wiley-VCH GmbH

neat PBTTT, which promotes a favorable morphology, that is, one that assures long-range electrical connectivity and low disorder. As a summary of this section, we propose that both things, namely aligned energy levels and a high degree of connectivity effect, are needed in order to improve the performance of blends with respect to the pristine material.

3. Conclusions

We have demonstrated that polymer mixtures of PBTTT with P3HT have outstanding thermoelectric properties, with $zT \approx 0.1$. The achieved electrical conductivity and Seebeck coefficient are comparable to films processed through other, more complex processing methods that produce uniaxially oriented samples or samples with domains that are well aligned over large length scales. The improved thermoelectric properties are explained by a combined effect of induced-ordering, driven by the guest material, and a finely tuned energy landscape. By investigating blends of PBTTT as a host material with guest materials P3HT, PCBM, PFO, PTB7-Th, PCDTBT, PCPDTBT, PBDB-T, PBDB-2F, and PBDB-2Cl, we conclude that the two requirements for the guest material to result in improvement of the thermoelectric power factor are having a high degree of electrical connectivity between domains and, simultaneously, HOMO energy levels close to that of the host material.

4. Experimental Section

Materials and Sample Preparation: PBTTT-C14 (M_w = 50 kDa; 1-Material) here referred to as PBTTT for simplicity, PTB7-Th (140 kDa, Ossila), F4TCNQ (from TCI-Chemicals), PCPDTBT (30 kDa, Sigma-Aldrich), PCDTBT (34 kDa, Sigma-Aldrich), PFO (80.9 kDa, Ossila), PBDB-T (90 kDa, Ossila), PBDB-2F (107 kDa, Ossila), and PBDB-2Cl (77 kDa, Ossila) were used as received. Chlorobenzene (>99%) was purchased from Sigma-Aldrich. Polymer films were fabricated from 20 mg mL^{-1} solutions in chlorobenzene. Solutions were stirred for 3 h at 110 °C. Polymer blends were prepared from dilutions of their respective stock polymer solutions using the same stirring conditions. As substrates, microscope glass slides were used from LabBox. Before deposition, they were cleaned using consecutive sonication baths of 10 min in a Hellmanex solution diluted at 10 vol% in water and isopropanol. Finally, they were dried using an air-flow and processed in a UVO-cleaner for 5 min. Films were deposited under nitrogen atmosphere using a preheated blade coater at 110 °C, with a blade height of 200 µm and a speed of 30 mm s^{-1}. Alternatively, films with a thickness gradient were fabricated by continuously varying the deposition speed.[46] A small subset of films was fabricated by spin coating for comparison. All films were precrystallized at 180 °C, under a nitrogen atmosphere for 15 min. The only exception was PBTTT in the ribbon phase, which was annealed at 270 °C. For doping, a vapor-phase methodology described in detail in ref. [10] was employed. Films with a thickness gradient were sectioned with a knife so that the area of each measured sample was approximately 20 mm × 2 mm. The area of the homogeneous films was 18 mm × 16 mm. As electronic contacts, silver paint was employed at the four corners. Alternatively, films used for GIWAXS characterization were fabricated using the same thermal annealing and doping methodology but using a spin coating technique and silicon substrates.

Characterization: UV–vis–NIR spectra were measured by using a Bruker HYPERION Fourier transform infrared spectroscopy (FTIR) microscope connected to a VERTEX 70 spectrometer. The Seebeck coefficient and electrical conductivity were measured using a custom-built setup described in a previous publication.[25] AFM experiments were done with a Keysight 5500 LS system. GIWAXS analysis was conducted at the BL11 non crystalline difraction (NCD)-SWEET beamline at ALBA Synchrotron Radiation Facility (Spain). The films were illuminated for 5 s with an X-ray beam of 12.4 keV at an angle of incidence of 0.12°. Scattering patterns were acquired using a Rayonix LX255-HS detector, positioned at a distance of 200.9 mm from the samples. The thickness of the deposited samples was determined by using a P16+ profilometer from KLA Tencor. Raman was collected using a Witec Alpha300RA equipment exciting with a 488 nm solid state laser. Fast scanning calorimetry was measured using Mettler Toledo Flash DSC +1. Thermal conductivity measurements were done using the Frequency Domain Thermo Reflectance method in a custom-built setup. Further description of the method and the measurement is available in Figure S16 in the Supporting Information.

Supporting Information

Supporting Information is available from the Wiley Online Library or from the author.

Acknowledgements

The authors acknowledge financial support from the Spanish Ministry of Science and Innovation through the Severo Ochoa" Program for Centers of Excellence in R&D (No. CEX2019-000917-S) and projects PGC2018-095411- B-I00, PGC2018-094620-A-I00, and MAT2017-90024-P (TANGENTS)-EI/Fondo Europeo de Desarrollo Regional and from the European Research Council (ERC) under Grant Agreements Nos. 648901 and 963954. J.M. thanks Ministerio de Ciencia, Innovación y Universidades for the Ramón y Cajal contract. The authors are thankful to Dr. Agustín Mihi for access and support with the FTIR equipment. The authors acknowledge the European funding (European Regional Development Fund and European Social Fund). The authors thank Andrés Gómez Rodríguez from the Scanning Probe Microscopy Laboratory (ICMAB-CSIC) for a set of fine AFM measurements. GIWAXS experiments were performed at NCD-SWEET beamline at ALBA Synchrotron with the collaboration of ALBA staff. Finally, the authors acknowledge the support of the publication fee by the CSIC Open Access Publication Support Initiative through its Unidad de Recursos de Información Científica para la Investigación (URICI). M.K. thanks the Carl Zeiss Foundation for financial support. G.Z. acknowledges the support from Alexander von Humboldt Foundation.

Conflict of Interest

The authors declare no conflict of interest.

Data Availability Statement

The data that support the findings of this study are available from the corresponding author upon reasonable request.

Keywords

doping, microstructure, organic thermoelectrics, orientation, ternary

Received: December 31, 2021
Revised: February 23, 2022
Published online: April 7, 2022

© 2022 The Authors. Advanced Energy Materials published by Wiley-VCH GmbH

[1] A. Hamidi-Sakr, L. Biniek, J.-L. L. Bantignies, D. Maurin, L. Herrmann, N. Leclerc, P. Lévêque, V. Vijayakumar, N. Zimmermann, M. Brinkmann, *Adv. Funct. Mater.* **2017**, *27*, 1700173.
[2] L. Biniek, S. Pouget, D. Djurado, E. Gonthier, K. Tremel, N. Kayunkid, E. Zaborova, N. Crespo-Monteiro, O. Boyron, N. Leclerc, S. Ludwigs, M. Brinkmann, *Macromolecules* **2014**, *47*, 3871.
[3] D. Scheunemann, V. Vijayakumar, H. Zeng, P. Durand, N. Leclerc, M. Brinkmann, M. Kemerink, *Adv. Electron. Mater.* **2020**, *6*, 2000218.
[4] D. M. DeLongchamp, R. J. Kline, Y. Jung, D. S. Germack, E. K. Lin, A. J. Moad, L. J. Richter, M. F. Toney, M. Heeney, I. McCulloch, *ACS Nano* **2009**, *3*, 780.
[5] J. Sun, M.-L. L. Yeh, B. J. Jung, B. Zhang, J. Feser, A. Majumdar, H. E. Katz, *Macromolecules* **2010**, *43*, 2897.
[6] G. D. Mahan, J. O. Sofo, *Proc. Natl. Acad. Sci. USA* **1996**, *93*, 7436.
[7] G. Zuo, X. Liu, M. Fahlman, M. Kemerink, *Adv. Funct. Mater.* **2018**, *28*, 1703280.
[8] A. Abtahi, S. Johnson, S. M. Park, X. Luo, Z. Liang, J. Mei, K. R. Graham, *J. Mater. Chem. A* **2019**, *7*, 19774.
[9] G. Zuo, X. Liu, M. Fahlman, M. Kemerink, *ACS Appl. Mater. Interfaces* **2018**, *10*, 9638.
[10] O. Zapata-Arteaga, B. Dörling, A. Perevedentsev, J. Martín, J. S. Reparaz, M. Campoy-Quiles, N. Dörling, A. Perevedentsev, J. Martín, J. S. Reparaz, M. Campoy-Quiles, *Macromolecules* **2020**, *53*, 609.
[11] O. Zapata-Arteaga, A. Perevedentsev, S. Marina, J. Martin, J. S. Reparaz, M. Campoy-Quiles, *ACS Energy Lett.* **2020**, *5*, 2972.
[12] A. M. Glaudell, J. E. Cochran, S. N. Patel, M. L. Chabinyc, *Adv. Energy Mater.* **2015**, *5*, 1401072.
[13] Z. Liang, H. H. Choi, X. Luo, T. Liu, A. Abtahi, U. S. Ramasamy, J. A. Hitron, K. N. Baustert, J. L. Hempel, A. M. Boehm, A. Ansary, D. R. Strachan, J. Mei, C. Risko, V. Podzorov, K. R. Graham, *Nat. Mater.* **2021**, *20*, 518.
[14] O. Bubnova, Z. U. Khan, A. Malti, S. Braun, M. Fahlman, M. Berggren, X. Crispin, *Nat. Mater.* **2011**, *10*, 429.
[15] N. C. Miller, R. Gysel, C. E. Miller, E. Verploegen, Z. Beiley, M. Heeney, I. McCulloch, Z. Bao, M. F. Toney, M. D. McGehee, *J. Polym. Sci., Part B: Polym. Phys.* **2011**, *49*, 499.
[16] N. C. Miller, E. Cho, M. J. N. N. Junk, R. Gysel, C. Risko, D. Kim, S. Sweetnam, C. E. Miller, L. J. Richter, R. J. Kline, M. Heeney, I. McCulloch, A. Amassian, D. Acevedo-Feliz, C. Knox, M. R. Hansen, D. Dudenko, B. F. Chmelka, M. F. Toney, J.-L. L. Brédas, M. D. McGehee, *Adv. Mater.* **2012**, *24*, 6071.
[17] B. Neelamraju, K. E. Watts, J. E. Pemberton, E. L. Ratcliff, *UTC* **2018**, *9*, 6871.
[18] S. N. Patel, A. M. Glaudell, K. A. Peterson, E. M. Thomas, K. A. O'Hara, E. Lim, M. L. Chabinyc, *Sci. Adv.* **2017**, *3*, e1700434.
[19] H. Hase, K. O'Neill, J. Frisch, A. Opitz, N. Koch, I. Salzmann, K. O'Neill, J. Frisch, A. Opitz, N. Koch, I. Salzmann, K. O'Neill, J. Frisch, A. Opitz, N. Koch, I. Salzmann, *J. Phys. Chem. C* **2018**, *122*, 25893.
[20] I. E. Jacobs, C. Cendra, T. F. Harrelson, Z. I. Bedolla Valdez, R. Faller, A. Salleo, A. J. Moulé, *Mater. Horiz.* **2018**, *5*, 655.
[21] H. Méndez, G. Heimel, S. Winkler, J. Frisch, A. Opitz, K. Sauer, B. Wegner, M. Oehzelt, C. Röthel, S. Duhm, D. Többens, N. Koch, I. Salzmann, *Nat. Commun.* **2015**, *6*, 8560.
[22] D. T. Duong, C. Wang, E. Antono, M. F. Toney, A. Salleo, *Org. Electron.* **2013**, *14*, 1330.
[23] V. Vijayakumar, Y. Zhong, V. Untilova, M. Bahri, L. Herrmann, L. Biniek, N. Leclerc, M. Brinkmann, *Adv. Energy Mater.* **2019**, *9*, 1900266.
[24] V. Vijayakumar, E. Zaborova, L. Biniek, H. Zeng, L. Herrmann, A. Carvalho, O. Boyron, N. Leclerc, M. Brinkmann, *ACS Appl. Mater. Interfaces* **2019**, *11*, 4942.
[25] B. Dörling, O. Zapata-Arteaga, M. Campoy-Quiles, *Rev. Sci. Instrum.* **2020**, *91*, 105111.
[26] D. M. Delongchamp, R. J. Kline, Y. Jung, E. K. Lin, D. A. Fischer, D. J. Gundlach, S. K. Cotts, A. J. Moad, L. J. Richter, M. F. Toney, M. Heeney, I. McCulloch, *Macromolecules* **2008**, *41*, 5709.
[27] I. McCulloch, M. Heeney, C. Bailey, K. Genevicius, I. MacDonald, M. Shkunov, D. Sparrowe, S. Tierney, R. Wagner, W. Zhang, M. L. Chabinyc, R. J. Kline, M. D. McGehee, M. F. Toney, *Nat. Mater.* **2006**, *5*, 328.
[28] D. M. DeLongchamp, R. J. Kline, E. K. Lin, D. A. Fischer, L. J. Richter, L. A. Lucas, M. Heeney, I. McCulloch, J. E. Northrup, *Adv. Mater.* **2007**, *19*, 833.
[29] M. L. Chabinyc, M. F. Toney, R. J. Kline, I. McCulloch, M. Heeney, *J. Am. Chem. Soc.* **2007**, *129*, 3226.
[30] T. Schuettfort, B. Watts, L. Thomsen, M. Lee, H. Sirringhaus, C. R. McNeill, *ACS Nano* **2012**, *6*, 1849.
[31] M. J. Lee, D. Gupta, N. Zhao, M. Heeney, I. McCulloch, H. Sirringhaus, *Adv. Funct. Mater.* **2011**, *21*, 932.
[32] X. Xue, G. Chandler, X. Zhang, R. J. Kline, Z. Fei, M. Heeney, P. J. Diemer, O. D. Jurchescu, B. T. O'Connor, *ACS Appl. Mater. Interfaces* **2015**, *7*, 26726.
[33] N. F. A. Zainal, C. H. Chan, in *Compatibilization of Polymer Blends*, (Eds: A. R. Ajitha, S. Thomas), Elsevier, New York **2020**, pp. 391–433.
[34] J. P. Penning, R. St J Manley, *Macromolecules* **1996**, *29*, 77.
[35] E. Lim, K. A. Peterson, G. M. Su, M. L. Chabinyc, *Chem. Mater.* **2018**, *30*, 998.
[36] D. T. Scholes, S. A. Hawks, P. Y. Yee, H. Wu, J. R. Lindemuth, S. H. Tolbert, B. J. Schwartz, *J. Phys. Chem. Lett.* **2015**, *6*, 4786.
[37] E. Lim, A. M. Glaudell, R. Miller, M. L. Chabinyc, *Adv. Electron. Mater.* **2019**, *5*, 1800915.
[38] K. Kang, S. Watanabe, K. Broch, A. A. Sepe, A. Brown, I. Nasrallah, M. Nikolka, Z. Fei, M. Heeney, D. Matsumoto, K. Marumoto, H. Tanaka, S.-I. I. Kuroda, H. Sirringhaus, *Nat. Mater.* **2016**, *15*, 896.
[39] P. Y. Yee, D. T. Scholes, B. J. Schwartz, S. H. Tolbert, *J. Phys. Chem. Lett.* **2019**, *10*, 4929.
[40] M. Lepinoy, P. Limelette, B. Schmaltz, F. T. Van, *Sci. Rep.* **2020**, *10*, 8086.
[41] S. D. Kang, G. J. Snyder, S. Dongmin Kang, G. Jeffrey Snyder, *Nat. Mater.* **2017**, *16*, 252.
[42] S. A. Gregory, R. Hanus, A. Atassi, J. M. Rinehart, J. P. Wooding, A. K. Menon, M. D. Losego, G. J. Snyder, S. K. Yee, *Nat. Mater.* **2021**, https://doi.org/10.1038/s41563-021-01008-0.
[43] I. E. Jacobs, A. J. Moulé, *Adv. Mater.* **2017**, *29*, 1703063.
[44] I. E. Jacobs, E. W. Aasen, J. L. Oliveira, T. N. Fonseca, J. D. Roehling, J. Li, G. Zhang, M. P. Augustine, M. Mascal, A. J. Moulé, *J. Mater. Chem. C* **2016**, *4*, 3454.
[45] J. E. Cochran, M. J. N. Junk, J. S. Cowart, L. Miller, A. M. Glaudell, C. Liman, M. F. Toney, C. J. Hawker, B. F. Chmelka, M. L. Chabinyc, P. L. Miller, J. S. Cowart, M. F. Toney, C. J. Hawker, B. F. Chmelka, M. L. Chabinyc, *Macromolecules* **2014**, *47*, 6836.
[46] A. Sánchez-Díaz, X. Rodríguez-Martínez, L. Córcoles-Guija, G. Mora-Martín, M. Campoy-Quiles, *Adv. Electron. Mater.* **2018**, *4*, 1700477.

© 2022 The Authors. Advanced Energy Materials published by Wiley-VCH GmbH